ELSEVIER

Biochimica et Biophysica Acta 1372 (1998) 347–358

BIOCHIMICA ET BIOPHYSICA ACTA
BBA

Thermotropic behavior of galactosylceramides with *cis*-monoenoic fatty acyl chains[1]

Vitthal S. Kulkarni [2], Rhoderick E. Brown *

The Hormel Institute, University of Minnesota, 801 16th Avenue NE, Austin, MN 55912, USA

Received 10 February 1998; accepted 17 April 1998

Abstract

To define the thermotropic behavior of galactosylceramides (GalCer) containing *cis* monounsaturated acyl chains, *N*-X:$1^{\Delta(X-9)\ cis}$ galactosylsphingosines (GalSph) were synthesized (where $X = 24$, 22, 20, or 18) and investigated by differential scanning calorimetry (DSC). After hydration of dried glycolipid, aqueous dispersions were prepared by repetitive heating and freeze-thaw cycles. The DSC data clearly showed that introducing a single *cis* double bond into the acyl chain of GalCer lowers the transition temperature of the main endothermic peak and affects the kinetics of formation of various metastable and stable gel phases. More importantly, the data emphasize the role that double bond location in concert with acyl chain length play in modulating the thermotropic behavior of GalCers. In contrast to the 18:1 GalCer and 20:1 GalCer endotherms which remain unchanged after identical repetitive heating scans and low temperature incubations, the thermotropic responses of 22:1 GalCer and 24:1 GalCer depended directly upon incubation time at lower temperatures following a heating scan. Only after extended incubation (4–5 days) did the endotherms revert to behavior observed during the initial heating scan that followed sample preparation by cyclic heating and freeze-thaw methods. The extended incubation times required for 22:1 GalCer and 24:1 GalCer to assume their more stable packing motifs appear to be consistent with nucleation events that promote transbilayer interdigitation. Yet, due to the slow kinetics of the process, the presence of *cis* monounsaturation in very long acyl chains that are common to GalCer may effectively inhibit transbilayer lipid interdigitation under physiological conditions.

Keywords: Sphingolipid; Differential scanning calorimetry; Metastable phase formation; Hydrocarbon chain-length asymmetry; Human immunodeficiency virus glycolipid receptor

1. Introduction

Galactosylceramide (GalCer) is a glycosphingolipid that plays a key role in the HIV-1 infection pathway of cells which lack the CD4 protein receptor, i.e., neural and colonic cells [1,2]. In these cells, GalCer reportedly acts as a high-affinity receptor for the gp120 protein of HIV-1 [3,4]. The interaction between GalCer and gp120 appears to involve the V3 loop of the viral glycoprotein [5–8]. The V3 loop is postulated to control the fusion between the envelope

Abbreviations: DSC, differential scanning calorimetry; FTIR, Fourier transform infrared; GalCer or *N*-acyl GalSph, galactosylceramide; GalSpd, galactosylsphingoid; HIV, human immunodeficiency virus; NMR, nuclear magnetic resonance; TLC, thin layer chromatography

* Corresponding author. Fax: (507) 4379606; E-mail: reb@maroon.tc.umn.edu

[1] Portions of this investigation were presented at the 41st Annual Meeting of the Biophysical Society held in New Orleans, LA, USA [69].

[2] Present address: Department of Pathology, Yale University School of Medicine, 310 Cedar St., New Haven, CT 06520-8023, USA.

0005-2736/98/$19.00
PII: S0005-2736(98)00076-5

of HIV-1 and the target cell membranes. Aside from the receptor role in HIV-1 infection, GalCer also serves as a critical structural element in the membranes of certain specialized tissues. In intestinal brush border, granular epidermis, and myelin sheath, GalCer accounts for a substantial amount of the total lipid. In myelin, for instance, GalCer makes up 20% of the total lipid, but because of transmembrane asymmetry, mole fractions may approach 0.4 in the outer half of myelin bilayers [9]. The high GalCer levels are thought to endow myelin with the special features necessary to effectively insulate nerve fibers. However, if GalCer levels become deficient in concert with excess accumulation of galactosylsphingosine, as is the case in inherited pathological conditions such as globoid cell leukodystrophy, then disruption of normal membrane function occurs within afflicted cells [10]. Hence, the GalCer level found in normal myelin appears to be carefully regulated and optimally poised for maintaining the unusually low proton permeability of myelin [11]. Yet, exactly which of the structural features of GalCer is responsible for the interesting physico-chemical characteristics that this glycolipid imparts to membranes remains unclear.

Naturally occurring GalCer possesses a number of unusual physical properties compared to other membrane lipids [12–14]. This monoglycosylated sphingolipid has the capacity to form various gel-like bilayer phases in excess water including an extraordinarily stable, crystalline lamellar phase [15–20]. Interestingly, changing the *N*-fatty acyl chain of GalCer from palmitate (16:0) to stearate (18:0) or to lignocerate (24:0) has little effect on the main thermal phase transition temperature (approx. 82°C) or on the enthalpy of transition (approx. 15 kcal/mol) [16,18,20]. From FT-IR studies, multiple metastable, gel-like phases have been reported in bovine brain GalCer, providing the possibility for the coexistence of multiple lateral domains enriched in various GalCer species [21]. The interesting physical properties of GalCer are postulated to result from a combination of structural features including an uncharged, relatively non-bulky and poorly hydratable sugar headgroup [22,23], an abundance of very long, saturated acyl chains providing marked intramolecular chain-length asymmetry, significant levels of 2-hydroxylated acyl chains (e.g., [24]), and functional groups that can donate and accept hydrogen bonds with neighboring lipids [25–27].

Despite the abundance of long, saturated acyl chains in brain GalCer, over one-third of the non-hydroxylated acyl chains typically are *cis* monounsaturated, nervonoyl ($24{:}1^{\Delta 15(c)}$) residues [28]. This situation has prompted studies into the role of acyl chain unsaturation on GalCer's physical properties using various techniques including Langmuir film balance methods [29–34], NMR [33,34], X-ray diffraction [35,36], electron microscopy [37,38] and microcalorimetry [35,36]. However, investigations into the thermotropic behavior of GalCers with unsaturated acyl chains have been confined to chain lengths of 16 or 18 carbons [35,36]. The resulting data have revealed that introducing *cis* unsaturation into the acyl chain of GalCer markedly lowers the main endothermic transition temperature and affects the kinetics of formation of various metastable and stable phases. To determine the thermotropic behavior of GalCers that contain long monounsaturated acyl chains, we undertook the present differential scanning calorimetric (DSC) investigation. Our results show that the thermotropic behavior of GalCers with long-chain monoenoic acyl chains (e.g., $24{:}1^{\Delta 15(c)}$ and $22{:}1^{\Delta 13(c)}$) depends critically on incubation time and temperature prior to DSC scanning. The thermotropic response differs significantly from that obtained with GalCers containing shorter monoenoic acyl chains (e.g., $20{:}1^{\Delta 11(c)}$ or $18{:}1^{\Delta 9(c)}$).

2. Materials and methods

2.1. Synthesis of GalCers with homogeneous monoenoic acyl chains

Monoenoic fatty acids were purchased from Nu-Chek-Prep. (Elysian, MN). Other reagents were purchased from Sigma-Aldrich. *N*-Acylated galactosylsphingosines with fatty acyl residues consisting of $24{:}1^{\Delta 15(c)}$ (nervonate), $22{:}1^{\Delta 13(c)}$ (erucate), $20{:}1^{\Delta 11(c)}$ (eicosenoate), or $18{:}1^{\Delta 9(c)}$ (oleate) were synthesized and purified as described previously [31,38]. Briefly, the *N*-hydroxysuccinimide ester of the desired fatty acid was prepared, recrystallized, and reacted with psychosine (lyso-GalCer) which had been produced by alkaline de-acylation of bovine brain GalCer.

Thin layer chromatographic (TLC) analysis using $CHCl_3/CH_3OH/NH_4OH$ (6:3:0.5) revealed that the lyso-GalCer contained mostly the sphingosine (>98%) rather than the dihydrosphingosine base. The resulting *N*-acyl GalSphs were purified by flash column chromatography, and recrystallized from −20°C acetone. Lipid purity and *N*-acyl homogeneity were confirmed by TLC and capillary gas chromatography, respectively, as described previously [38].

2.2. Lipid dispersion preparation

Lipid dispersions were prepared in phosphate buffer (pH 6.6) containing 10 mM potassium phosphate, 100 mM sodium chloride, and 1.5 mM sodium azide [38]. Briefly, phosphate buffer was added to the vacuum-dried lipid which was then incubated above 90°C for 3 min, vortexed vigorously, and briefly bath sonicated (above 90°C). This process was repeated two more times. Then, the dispersion was subjected to three freeze-thaw cycles to obtain a uniform distribution of buffer solutes across the bilayers [39]. Rapid freezing was achieved by immersing the lipid suspension in an isopropanol bath cooled by dry ice. During each thawing cycle, the glycolipid dispersion was raised above 90°C and vortexed prior to subsequent freezing. Lipid dispersions were degassed before loading into the microcalorimeter cell and incubated at 4°C for 3 h prior to initiating the first heating scan.

2.3. Differential scanning calorimetry

All thermotropic scans were obtained using a high-sensitivity MC-2 differential scanning calorimeter (Microcal, Amherst, MA) equipped with a DT-2801 data acquisition board for automated and computer controlled data collection. The microcalorimeter was calibrated using three different high purity phospholipids (e.g., dimyristoyl phosphatidylcholine (DMPC), dipalmitoyl phosphatidylcholine (DPPC), and dibehenyl phosphatidylcholine (DBPC)) which have established phase transition features encompassing the range of 23–73°C [40]. The calibration was checked periodically. The heat capacity (cal/°C) versus temperature output of the reference buffer was subtracted from that of the samples and then normalized for the lipid concentration using the ORIGIN data analysis package (Microcal, Amherst, MA). Transition temperatures (T_m) and enthalpies (ΔH) were determined from the mid-point of and by integrating the peak area, respectively.

3. Results

3.1. Thermotropic behavior of N-24:1$^{\Delta 15}$ GalSph

Fig. 1 shows the thermotropic behavior of *N*-24:1$^{\Delta 15}$ GalSph aqueous dispersions obtained after incubating in various ways prior to scanning. The *N*-24:1$^{\Delta 15}$ GalSph dispersions were initially prepared by the freeze-thaw and heating protocol described in Section 2. All thermograms depict heating mode scans performed at a rate of 10°C/h. The first heating scans of freshly prepared dispersions of *N*-24:1$^{\Delta 15}$ GalSph invariably showed a major endothermic peak centered at approx. 67°C with an enthalpy (ΔH) of 14.4 kcal/mol (Fig. 1_A). However, this enthalpy value must be viewed as an approximation because of the endotherm's slightly non-symmetrical shape, which suggests the possibility of a second minor component centered near 64.2°C. Subsequent scans, in which samples were equilibrated at 4°C for 100 min before starting the scans, showed two distinct endothermic peaks (Fig. 1_C). One peak was centered at 58.4°C and a second peak was centered at 64.2°C. Accurate assessment of the molar enthalpies of each of these two endothermic peaks was not possible due to their simultaneous occurrence along with the known influence of lipid mesomorphic aggregation state on thermotropic properties. The 67°C high-enthalpy transition peak observed in Fig. 1_A completely disappeared (Fig. 1_C). This result was consistent with our earlier observation in which dual transition peaks were reported for *N*-24:1$^{\Delta 15}$ GalSph that had been subjected to multiple heating scans with relatively short equilibration times (1–2 h) between scans [38].

Heating scans obtained after incubating the same dispersions at room temperature (23 ± 0.5°C) for a minimum of 5 days showed a major endothermic peak at approx. 67°C (Fig. 1_D) which was very similar in shape and in total enthalpy to the initial scan of freshly prepared dispersions (Fig. 1_A). Heating

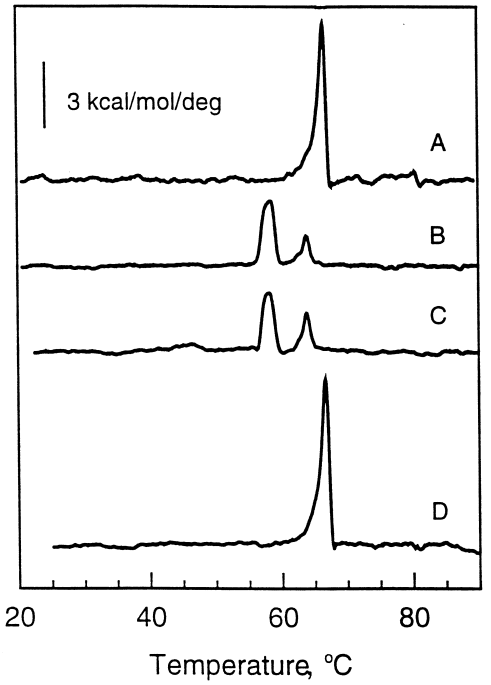

Fig. 1. DSC thermotropic behavior of 24:1 GalCer. All traces represent heating scans run at a rate of 10°C/h. Glycolipid aqueous dispersions were produced by the freeze-thaw and heat cycling protocol described in Section 2. (A) Freshly prepared 24:1 GalCer dispersion incubated for 3 h at 4°C prior to initiating the heating scan; (B) 24:1 GalCer dispersion incubated for 3 days at 22°C following an initial heating scan as described in A; (C) 24:1 GalCer dispersion incubated for 100 min at 4°C following an initial heating scan as described in A; (D) 24:1 GalCer dispersion incubated for 5 days at 22°C following an initial heating scan as described in A.

scans of *N*-24:1$^{\Delta 15}$ GalSph dispersions equilibrated for less than 5 days at room temperature (e.g., 4 days or 3 days) resulted in two peaks (e.g., Fig. 1_B) which were similar (T_m and ΔH) to the thermograms observed after short incubation times (2 h) at 4°C (Fig. 1_C). A somewhat similar pattern of metastable behavior also has been reported for the 24:1$^{\Delta 15}$ derivative of sulfated GalCer [70].

3.2. Thermotropic behavior of *N*-22:1$^{\Delta 13}$ GalSph

The thermotropic behavior of aqueous dispersions of *N*-22:1$^{\Delta 13}$ GalSph, prepared by the same freeze-thaw and heating procedure as used for *N*-24:1$^{\Delta 15}$ GalSph (see Section 2), is shown in Fig. 2. The initial heating scans obtained at 10°C/h showed an endotherm with a main phase transition temperature at 59°C along with a shoulder peak at 60°C. The total enthalpy was approx. 5.8 kcal/mol (Fig. 2_A). Subsequent heating scans obtained after incubating the *N*-22:1$^{\Delta 13}$ GalSph dispersions at 4°C for 100 min revealed a dramatic increase in complexity of the melting behavior (Fig. 2_B). Two new endothermic transition peaks were evident at approx. 52.2°C and at approx. 56.4°C. The latter peak overlapped with the main 59°C peak noted in Fig. 2_A. Also, there was a clear indication of an exothermic peak near 36.5°C. Interestingly, subsequent heating scans obtained after incubating these same dispersions at room temperature (23°C ± 0.5) for 3 days (Fig. 2_C) showed a reversion to the behavior originally observed following freeze-thaw preparation of *N*-22:1$^{\Delta 13}$ GalSph aqueous dispersions (Fig. 2_A), i.e., a major endothermic peak at 59°C along with the shoulder peak at 60°C (total $\Delta H = 6.1$ kcal/mol). Also, peak characteristics similar to those in Fig. 2_C were obtained after incubating for five instead of 3 days (data not shown).

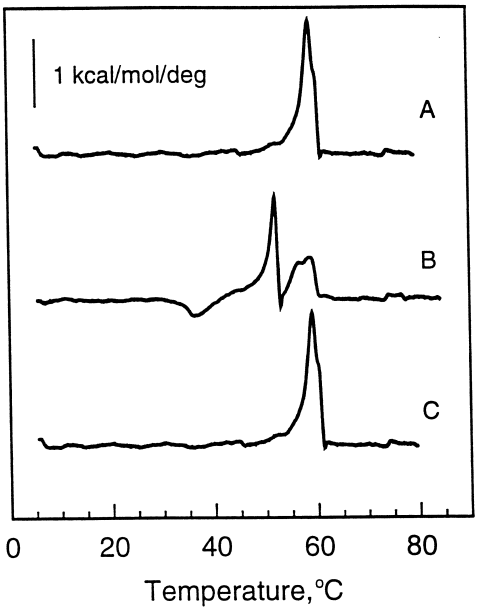

Fig. 2. DSC thermotropic behavior of 22:1 GalCer. All traces represent heating scans run at a rate of 10°C/h. Glycolipid aqueous dispersions were produced by the freeze-thaw and heat cycling protocol described in Section 2. (A) Freshly prepared 22:1 GalCer dispersion incubated for 3 h at 4°C prior to initiating the heating scan; (B) 22:1 GalCer dispersion incubated for 100 min at 4°C following an initial heating scan as described in A; (C) 22:1 GalCer dispersion incubated for 3 days at 22°C following an initial heating scan as described in A.

Hence, in many ways, the thermotropic behavior of *N*-22:1$^{\Delta 13}$ GalSph and *N*-24:1$^{\Delta 15}$ GalSph paralleled one another when subjected to similar thermal histories. Neither of these glycolipids was able to revert to their highest melting phase state(s) (achieved by freeze-thaw and thermal cycling) unless incubated for extended times at 23°C ± 0.5. In the case of *N*-22:1$^{\Delta 13}$ GalSph, a minimum of 3 days at 23°C was necessary; while for *N*-24:1$^{\Delta 15}$ GalSph, 5 days at 23°C was required.

Nonetheless, important differences in thermal behavior patterns of *N*-24:1$^{\Delta 15}$ GalSph and of *N*-22:1$^{\Delta 13}$ GalSph were evident. For instance, with *N*-24:1$^{\Delta 15}$ GalSph, the shorter-term incubations (e.g., 100 min at 4°C) resulted in two lower-temperature, endothermic peaks one of which appeared to correspond to the low-enthalpy 64.2°C shoulder component on the original high-enthalpy 67°C transition peak. Moreover, of the two lower-temperature peaks, the one with the lower melt temperature had the higher enthalpy. In contrast, of the endothermic peaks produced by the shorter term incubations of *N*-22:1$^{\Delta 13}$ GalSph, two appeared to be new lower-temperature peaks (e.g., 53°C and 56.4°C peaks) while one appeared to be a remnant of the original main 59°C peak. However, the high temperature shoulder at 60°C was not evident on this remnant peak.

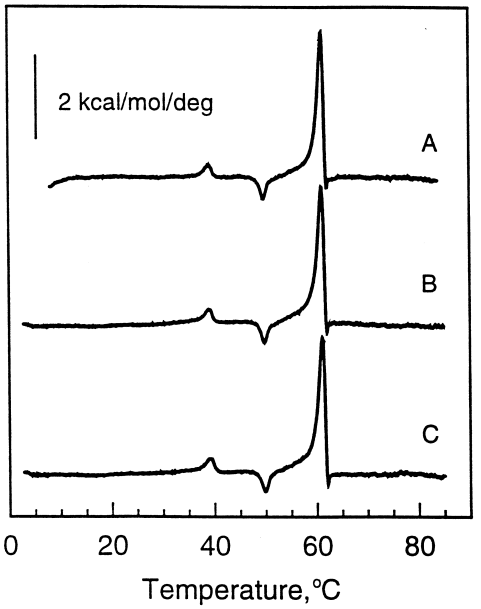

Fig. 3. DSC thermotropic behavior of 20:1 GalCer. All traces represent heating scans run at a rate of 10°C/h. Glycolipid aqueous dispersions were produced by the freeze-thaw and heat cycling protocol described in Section 2. (A) Freshly prepared 20:1 GalCer dispersion incubated for 3 h at 4°C prior to initiating the heating scan; (B) 20:1 GalCer dispersion incubated for 100 min at 4°C following an initial heating scan as described in A; (C) 20:1 GalCer dispersion incubated for 4 days at 22°C following an initial heating scan as described in A.

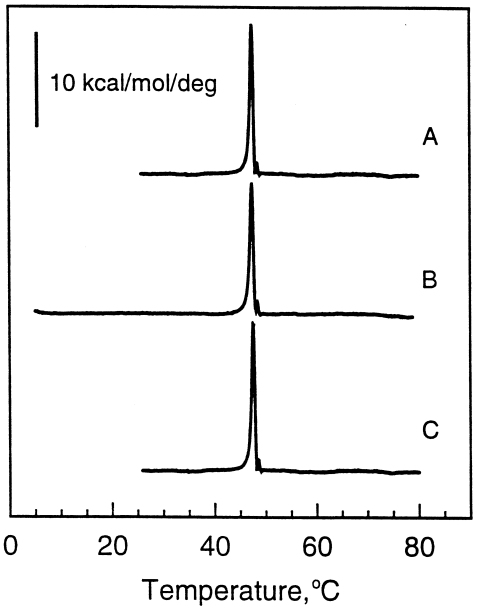

Fig. 4. DSC thermotropic behavior of 18:1 GalCer. All traces represent heating scans run at a rate of 10°C/h. Glycolipid aqueous dispersions were produced by the freeze-thaw and heat cycling protocol described in Section 2. (A) Freshly prepared 18:1 GalCer dispersion incubated for 3 h at 4°C prior to initiating the heating scan; (B) 18:1 GalCer dispersion incubated for 100 min at 4°C following an initial heating scan as described in A; (C) 18:1 GalCer dispersion incubated for 4 days at 22°C following an initial heating scan as described in A.

3.3. Thermotropic behavior of *N*-20:1$^{\Delta 11}$ GalSph

The thermotropic behavior of aqueous dispersions of *N*-20:1$^{\Delta 11}$ GalSph, prepared by the freeze-thaw procedure, is shown in Fig. 3. The behavior of *N*-20:1$^{\Delta 11}$ GalSph differs markedly from that of *N*-24:1$^{\Delta 15}$ GalSph and *N*-22:1$^{\Delta 13}$ GalSph. All heating scans obtained at 10°C/h were identical irrespective of thermal history or incubation conditions. For instance, when subjected to the same thermal cycling conditions as *N*-24:1$^{\Delta 15}$ GalSph or *N*-22:1$^{\Delta 13}$ GalSph, *N*-20:1$^{\Delta 11}$ GalSph dispersions always showed a main phase transition at 61.4°C with an

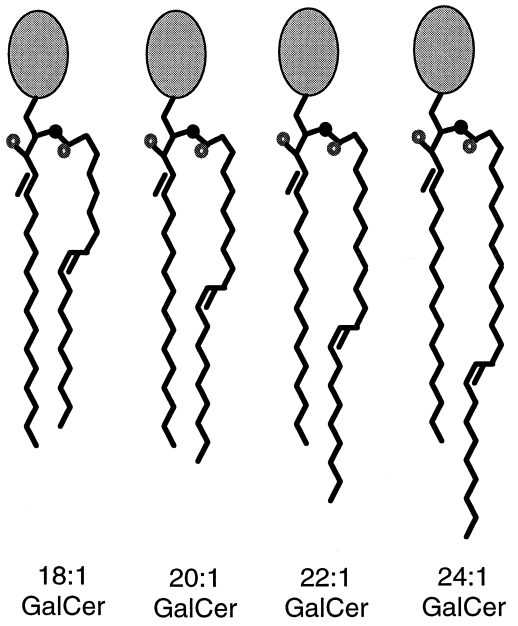

Fig. 5. Schematic representation of GalCer derivatives with monounsaturated acyl chains illustrating the possibilities for transbilayer hydrocarbon interdigitation. Hydrocarbon conformations are based on the NMR, diffraction, and MM3 modeling studies referred to in the text. For simplicity, long axis molecular tilt and headgroup conformation are not depicted although diffraction data and MM3 modeling data indicate that a bent 'shovel' conformation is likely in the stable gel phase in which the headgroup lies roughly parallel to the interfacial plane for GalCer lamellar crystalline phase(s) [48,67,68]. The transition from the liquid-crystalline phase to the stable gel phase leads to reorientation of the galactose [68]. In the schematic, the small black filled circle represents nitrogen and the small unfilled circle represents oxygen. Based on these conformational models, partial interdigitation of the hydrocarbon chains would be predicted for 24:1 GalCer and 22:1 GalCer, but not 20:1 GalCer or 18:1 GalCer.

approximate enthalpy of 7.3 kcal/mol. Two other minor thermally induced transitions also were evident. One was an endothermic peak centered at 39.1°C while the second was an exothermic peak centered at 50°C. As mentioned previously, absolutely accurate assessment of the molar enthalpies of each of these endothermic peaks was not possible due to their simultaneous occurrence along with the known influence of lipid mesomorphic aggregation state on thermotropic properties. Fig. 3_A shows the initial heating scan obtained after preparation of *N*-$20{:}1^{\Delta 11}$ GalSph. Fig. 3_B shows a subsequent heating scan obtained after incubating at 4°C for 100 min. Fig. 3_C shows a heating scan obtained after extended incubation (4 days or more) at room temperature.

3.4. Thermotropic behavior of *N*-$18{:}1^{\Delta 9}$ GalSph

Fig. 4 shows the heating scans (10°C/h) of aqueous dispersions of *N*-$18{:}1^{\Delta 9}$ GalSph prepared by the same freeze-thaw procedure used throughout this study. As with *N*-$20{:}1^{\Delta 11}$ GalSph, subjecting the *N*-$18{:}1^{\Delta 9}$ GalSph dispersions to the same thermal history as the other GalCer derivatives produced heating thermograms that all were identical. In the case of *N*-$18{:}1^{\Delta 9}$ GalSph, the first heating scan as well as subsequent heating scans obtained after incubating the lipid dispersion at 4°C for 100 min were identical (Fig. $4_{A,B}$). A main phase transition was evident at 47.7°C ($\Delta H = 14.6$ kcal/mol). Extended incubation of *N*-$18{:}1^{\Delta 9}$ GalSph (>4 days) at room temperature produced no change in the position of the main transition peak or in the transition enthalpy (Fig. 4_C).

4. Discussion

Among sphingoid-based lipids, existing thermotropic data is confined largely to sphingolipids having saturated *N*-acyl chains. Upon excess hydration, GalCers with *N*-acyl chains consisting of 16:0, 18:0 or 24:0 display major endothermic transitions confined to the 82–84°C range, whereas sphingomyelins with *N*-acyl chains consisting of 16:0, 18:0, 20:0, 22:0 or 24:0 have endothermic transitions with midpoints ranging from 40 to 47°C (for recent review, see [41]). The focus on sphingolipid species containing saturated acyl chains undoubtedly reflects the fact that sphingolipids isolated from natural sources often possess high levels of saturated acyl chains. Nonetheless, many naturally occurring sphingolipids also contain unsaturated acyl chains which typically are monoenoic and can account for a substantial amount of the total acyl composition. As was pointed out in Section 1, the nervonoyl (24:1) species makes up a significant fraction of the GalCer in myelin. This same acyl chain is found in high levels (30–40%) in the sphingomyelin of aging human lens tissue [42]. Also, drugs such as clofibrate cause a relative enrichment of sphingolipid species with 22:1 and 24:1 acyl chains compared to their saturated coun-

terparts in mouse liver [43]. However, the monounsaturated acyl chains of natural sphingolipids are not limited to long-chain residues. GalCers in human plasma and unfertilized chicken egg yolks contain 25–30% oleoyl chains [44,45]. Similar levels of GalCers with oleoyl residues reportedly occur in human aorta and increase relative to species with saturated acyl chains in atherosclerotic disease conditions involving fibrous plaques and lesions [46].

To date, investigations of the effects of acyl unsaturation on GalCer thermotropic behavior have been limited to HPLC-purified GalCers with moderate acyl heterogeneity [18] and to two studies involving GalCer with homogeneous 18-carbon or 16-carbon acyl chains [35,36]. From these studies, it is clear that introducing a single *cis* double bond into the acyl chain of GalCer lowers the transition temperature of the main endothermic peak and affects the kinetics of formation of various metastable and stable phases. Our data support these earlier findings but emphasize the role that double bond location in concert with acyl chain length play in modulating the thermotropic behavior of GalCers.

4.1. 18:1 GalCer behavior

Our *N*-18:1$^{\Delta 9}$ GalSph data show a dramatic lowering of the main endothermic transition peak (T_m of 47.7°C; ΔH = 14.6 kcal/mol). This finding agrees well with previous values (T_m = 44.8°C; ΔH = 11.5 kcal/mol) obtained on *N*-18:1$^{\Delta 9}$ GalSph hydrated to 70% in double-distilled water and using much faster scan rates (300°C/h) [35]. Interestingly, we found no change in subsequent heating scans of *N*-18:1$^{\Delta 9}$ GalSph whether incubated for 100 min at 4°C or for 4 days at 24°C after the initial heating scan. Again, these results agree with the findings of Reed and Shipley [35] who found the main endothermic transition peak to remain near 45°C if *N*-18:1$^{\Delta 9}$ GalSpd was cooled and incubated at temperatures below the 45–55°C range. However, Reed and Shipley [35] also noted a time-dependent transformation to a higher melting form (T_m of 55.5°C; ΔH = 12.1 kcal/mol), but only after a minimum of two incubations at temperatures between 45°C and 55°C. X-ray diffraction analyses revealed that both types of 'stable' low temperature phases packed into crystalline arrangements, but that the lower melting LC1 form had a reduced bilayer periodicity (56.5 Å) compared to the higher melting LC2 form (69.9 Å) [35]. The differences in bilayer periodicity presumably reflect chain tilt that occurs in the LC1, but not in the LC2 phase. In neither crystalline phase did the X-ray data suggest hydrocarbon interdigitation due to chain length asymmetry [35]. The transition that we observe for *N*-18:1$^{\Delta 9}$ GalSph (Fig. 4) appears to be the LC1 crystalline to L_α chain-melted transition previously characterized by Reed and Shipley [35].

The absence of hydrocarbon interdigitation in the low temperature phase(s) of *N*-18:1$^{\Delta 9}$ GalSph appears to be consistent with the accumulated structural and conformational data provided by NMR (e.g., [27,33,34,47]) and by diffraction data on related GalCer derivatives (e.g., [36,48]). The data indicates that the initial segment of the sphingosine base (carbons 1–5 and including the *trans* double bond between carbons 4 and 5) lies roughly orthogonal to the amide plane but with hydroxyl on carbon 3 oriented toward the hydrated interface [27]. The amide plane including the initial two carbons of the *N*-linked acyl chain extend roughly parallel to the bilayer interface but then the chain bends sharply to become parallel to the sphingosine chain (e.g., [49] and references therein). As a result, a positional inequivalence that affects the axial displacement of carbon atom positions exists along the two hydrocarbon chains. When the *N*-linked acyl chain contains a *cis* double bond, the axial displacement of some carbon atom positions will be exacerbated due to the 'crankshaft' type *trans-gauche* kink. A summary schematic is shown in Fig. 5. The situation is somewhat analogous to the more widely known positional inequivalence that occurs in the *sn*-1 and *sn*-2 chains of glycerol-based phospholipids [50].

4.2. 20:1 GalCer behavior

Changing the monounsaturated acyl chain of GalCer from 18:1$^{\Delta 9}$ to 20:1$^{\Delta 11}$ elevates the main endothermic transition temperature from 47.7°C to 61.4°C. However, given that the 47.7°C phase transition temperature for 18:1 GalCer probably reflects its metastable gel phase (LC1) to L_α chain-melted transition [35], it may be more appropriate to compare the 55.5°C stable gel phase (LC2) transition temperature of 18:1 GalCer [35] with the 61.4°C

transition temperature for 20:1 GalCer. The results are particularly interesting in light of the reported relative lack of sensitivity of GalCer's main endothermic transition temperature to changes in saturated acyl chain length. As mentioned previously, similar major endothermic transition temperatures (82–84°C) have been reported for GalCers with saturated acyl chains containing either 16, 18, or 24 carbons [16,20,35,38,51]. The lack of an effect of acyl chain length on the major transition temperature of GalCer coupled with the relatively high temperature of the transition often has been attributed to formation of a stable but less hydrated, crystalline packing state involving intermolecular hydrogen bonding (e.g., [25,26,52,53,68]). The presence of a *cis* double bond that increases sphingolipid average molecular cross-sectional area and disrupts chain-chain packing may facilitate hydration and diminish intermolecular hydrogen bonding interactions. As a result, the sphingolipid may become more responsive to changes in acyl chain length. Compared to 18:1 GalCer, the acyl chain region of 20:1 GalCer nearest to the sugar headgroup is lengthened by two carbons and the *cis* double bond is displaced away from the interfacial region but while remaining nine carbons from the terminal methyl group (Fig. 5). Hence, enhanced stabilization via van der Waals attractive forces could occur that leads to elevation of the main transition temperature (compared to 18:1 GalCer). Yet, the lowering of the main endothermic phase transition temperature of 20:1 GalCer by over 20°C relative to GalCers with saturated acyl chains shows that the *cis* double bond strongly diminishes the strength of the intermolecular interaction.

Indeed, the presence of a *cis* double bond in an acyl chain is known to introduce a 'crankshaft' type *trans-gauche* kink into the hydrocarbon chain [54]. Such a kink in the acyl chain of GalCer increases its average cross-sectional area (e.g., [29,31,55]) as well as the average intermolecular distance between molecules within each half of the bilayer. The net effect is to weaken intermolecular interactions and reduce the phase transition temperature.

4.3. 22:1 GalCer and 24:1 GalCer behavior

In 22:1 GalCer and 24:1 GalCer, the single endothermic phase transition peaks produced by freeze-thawing or by extended sample incubation at room temperature are centered near 59°C and 67°C, respectively. This suggests that, despite the Δ13 location in 22:1 GalCer and the Δ15 location in 24:1 GalCer, the *cis* double bonds must still disrupt the chain-ordered lamellar phase(s) that can occur in GalCer. Otherwise, transition peaks would be expected in the 82–84°C range where they have been reported for the 24:0, 18:0, and 16:0 derivatives of GalCer [20,35,38,51]. However, given that the midpoint of the main endothermic transition of 20:1 GalCer occurs at 61.4°C, it is appears that additional structural parameters impact on the behavior of 22:1 GalCer (and 24:1 GalCer). One possibility is that partial interdigitation occurs in 22:1 GalCer and 24:1 GalCer due to chain-length asymmetry. This possibility warrants consideration for several reasons. First, simple models based on the general conformational and configurational behavior of other GalCer derivatives (discussed previously) show that chain-length asymmetry is likely to occur in the chain-ordered phases of 22:1 GalCer and 24:1 GalCer, but not in those of 20:1 GalCer or 18:1 GalCer (Fig. 5). Secondly, chain-length inequivalence ratios ($\Delta C/CL$ ratios) calculated using the formalism developed by Huang and colleagues yield values consistent with partial interdigitation for 22:1 GalCer and 24:1 GalCer [56–58]. Assuming the occurrence of lamellar crystalline phases for 22:1 GalCer and for 24:1 GalCer, the $\Delta C/CL$ ratios are 0.26 and 0.34, respectively. Thirdly, based on X-ray diffraction data, Reed and Shipley [20] have reported that the major high-enthalpy transition of hydrated 24:0 GalCer is due to transformation from a partially interdigitated, chain-ordered, pseudocrystalline state to a chain-melted, liquid crystalline state. Similar findings have been reported for sulfated GalCer and sphingomyelin with 24:0 acyl chains below T_m [59–61]. Fourthly, the slight lowering of the main endothermic transition temperature of 22:1 GalCer ($T_m = 59$°C) relative to that of 20:1 GalCer ($T_m = 61.4$°C) appears to be consistent with thermotropic behavior known to occur in PCs in cases where interdigitation has been verified by diffraction or other structural approaches. In such systems, penetration of the relatively bulky terminal methyl groups of the longer hydrocarbon chains from one

lipid monolayer into the opposing monolayer induces a disordering effect ([62,63] and references therein). The disturbance reportedly is more pronounced when the terminal methyl groups remain close to the bilayer mid-plane. In comparing the behavior of 20:1 GalCer and 22:1 GalCer, it appears that the slight stabilizing effect expected by van der Waals forces from the increased hydrocarbon length of 22:1 GalCer may be compensated by the interdigitation expected for 22:1 GalCer but not for 20:1 GalCer. Taken together, the preceding four points suggest that chain-length interdigitation is a distinct possibility for 22:1 GalCer and 24:1 GalCer, given appropriate incubation conditions. However, our explanation for the thermotropic data must be viewed as tentative and will require further studies involving structural approaches to evaluate fully.

In contrast to the 18:1 GalCer and 20:1 GalCer endotherms which remain unchanged after identical repetitive heating scans and low temperature incubations employed for this study, the thermotropic responses of 22:1 GalCer and 24:1 GalCer depend directly upon incubation time at lower temperatures following a heating scan. With 22:1 GalCer and 24:1 GalCer, cooling and incubating at room temperature prior to rescanning yielded new lower-temperature endothermic peaks unless sample incubation is extended to 3 or more days (22:1 GalCer) or 5 or more days (24:1 GalCer). Only after extended incubation do the endotherms revert to responses originally observed during the initial heating scans that follow sample preparation by cyclic heating and freeze/thaw methods (Figs. 1 and 2). Presumably, the extended equilibration times allow the less stable phases of 22:1 GalCer and of 24:1 GalCer to convert to their thermodynamically more stable packing motifs which may require nucleation events that lead to transbilayer chain interdigitation. However, under physiological conditions, the presence of *cis* monounsaturation in the very long acyl chains that are common to GalCer may effectively inhibit interdigitation due to the slow kinetics of the process. The tendency for *cis* double bonds in acyl chains to inhibit transbilayer hydrocarbon chain interdigitation also has been suggested for sulfated GalCer derivatives [59]. In this way, *cis* monounsaturation in the very long acyl chains of sphingolipids may augment the effects of cholesterol which often concentrates in biomembranes that are relatively rich in sphingolipids and which interferes with their interdigitation [60,64].

Aside from the possible physiological relevance regarding the kinetic aspects of stable and metastable phase formation, GalCers with very long monounsaturated acyl chains also have shown promise in biotechnological applications involving the production of lipid nanotubes and related high-axial-ratio microstructures (e.g., [38,65,66]). Yet, it is becoming increasingly clear that formation of different mesomorphic aggregation states depends critically on production methodology including solvation, temperature, and incubation conditions. Hence, basic characterization and understanding of the physicochemical response(s) of such lipids take on added significance.

Acknowledgements

We thank Jan Smaby-Cook for assistance with the data analysis and presentation as well as Fred Phillips and Dr. Margot Cleary for their help with the capillary GC analyses of the glycolipid derivatives, and Carmen Hotson for secretarial services. The authors gratefully acknowledge the major support provided by USPHS Grant GM45928 and the Hormel Foundation.

References

[1] J.M. Harouse, S. Bhat, S.L. Spitalnik, M. Laughlin, K. Stefano, D.H. Silberberg, F. Gonzalez-Scarano, Inhibition of entry of HIV-1 in neural cell lines by antibodies against galactosyl ceramide, Science 253 (1991) 320–323.

[2] N. Yahi, S. Baghdiguian, H. Moreau, J. Fantini, Galactosylceramide (or a closely related molecule) is the receptor for human immunodeficiency virus type 1 on human colon epithelial HT29 cells, J. Virol. 66 (1992) 4848–4854.

[3] S. Bhat, S.L. Spitalnik, F. Gonzalez-Scarano, D.H. Silberberg, Galactosyl ceramide or a derivative is an essential component of the neural receptor for human immunodeficiency virus type 1 envelope glycoprotein gp120, Proc. Natl. Acad. Sci. USA 88 (1991) 7131–7134.

[4] D. Long, J.F. Berson, D.G. Cook, R.W. Doms, Characterization of human immunodeficiency virus type 1 gp120 binding to liposomes containing galactosylceramide, J. Virol. 68 (1994) 5890–5898.

[5] D.G. Cook, J. Fantini, S.L. Spitalnik, F. Gonzalez-Scarano, Binding of human immunodeficiency virus type 1 (HIV-1) gp120 to galactosylceramide (GalCer): relationship to the V3 loop, Virology 201 (1994) 206–214.
[6] N. Yahi, J. Sabatier, P. Nickel, K. Mabrouk, F. Gonzalez-Scarano, J. Fantini, Suramin inhibits binding of the V3 region of HIV-1 envelope glycoprotein gp120 to galactosylceramide, the receptor for HIV-1 gp120 on the human colon epithelial cells, J. Biol. Chem. 269 (1994) 24349–24353.
[7] N. Yahi, J. Sabatier, S. Baghdiguian, F. Gonzalez-Scarano, J. Fantini, Synthetic multimeric peptides derived from the principal neutralization domain (V3 loop) of human immunodeficiency virus type 1 (HIV-1) gp120 bind to galactosylceramide and block HIV-1 infection in a human CD-4 negative mucosal epithelial cell line, J. Virol. 69 (1995) 320–325.
[8] J. Fantini, D. Hammache, O. Delézay, N. Yahi, C. André-Barrès, I. Rico-Lattes, A. Lattes, Synthetic soluble analogs of galactosylceramide (GalCer) bind to the V3 domain of HIV-1 gp120 and inhibit HIV-1-induced fusion and entry, J. Biol. Chem. 272 (1997) 7245–7252.
[9] C. Linington, M.G. Rumsby, Accessibility of galactosyl ceramides to probe reagents in central nervous system myelin, J. Neurochem. 35 (1980) 983–992.
[10] L. Svennerholm, M.-T. Vanier, J.-E. Månsson, Krabbe disease: a galactosylsphingosine (psychosine) lipidosis, J. Lipid Res. 21 (1980) 53–64.
[11] R.S. Diaz, J. Monreal, Unusual low proton permeability of liposomes prepared from the endogenous myelin lipids, J. Neurochem. 62 (1994) 2022–2029.
[12] T.E. Thompson, T.W. Tillack, Organization of glycosphingolipids in bilayers and plasma membranes of mammalian cells, Annu. Rev. Biophys. Biophys. Chem. 14 (1985) 361–386.
[13] W. Curatolo, The physical properties of glycolipids, Biochim. Biophys. Acta 906 (1987) 111–136.
[14] B. Maggio, The surface behavior of glycosphingolipids in biomembranes: a new frontier of molecular ecology, Prog. Biophys. Mol. Biol. 62 (1994) 55–117.
[15] M.R. Bunow, Two gel states of cerebrosides: calorimetric and Raman spectroscopic evidence, Biochim. Biophys. Acta 574 (1979) 542–546.
[16] M.J. Ruocco, D. Atkinson, D.M. Small, R.P. Skarjune, E. Oldfield, G.G. Shipley, X-ray diffraction and calorimetric study of anhydrous and hydrated N-palmitoylgalactosylsphingosine (cerebroside), Biochemistry 20 (1981) 5957–5966.
[17] W. Curatolo, Thermal behavior of fractionated and unfractionated bovine brain cerebrosides, Biochemistry 21 (1982) 1761–1764.
[18] W. Curatolo, F.B. Jungalwala, Phase behavior of galactocerebrosides from bovine brain, Biochemistry 24 (1985) 6608–6613.
[19] D.C. Lee, I.R. Miller, D. Chapman, An infrared spectroscopic study of metastable and stable forms of hydrated cerebroside bilayers, Biochim. Biophys. Acta 859 (1986) 266–270.
[20] R.A. Reed, G.G. Shipley, Structure and metastability of N-lignocerylgalactosylsphingosine (cerebroside) bilayers, Biochim. Biophys. Acta 896 (1987) 153–164.
[21] M. Jackson, D.S. Johnston, D. Chapman, Differential scanning calorimetric and Fourier transform infrared spectroscopic investigations of cerebroside polymorphism, Biochim. Biophys. Acta 944 (1988) 497–506.
[22] M.J. Ruocco, G.G. Shipley, Hydration of *N*-palmitoylgalactosylsphingosine compared to monosaccharide hydration, Biochim. Biophys. Acta 735 (1983) 305–308.
[23] A. Sen, S.-W. Hui, Direct measurement of headgroup hydration of polar lipids in inverted micelles, Chem. Phys. Lipids 49 (1988) 179–184.
[24] S.B. Johnson, R.E. Brown, Simplified derivatization for determining sphingolipid fatty acyl composition by gas chromatography-mass spectrometry, J. Chromatogr. 605 (1992) 281–286.
[25] M.R. Bunow, I.W. Levin, Molecular conformations of cerebrosides in bilayers determined by Raman spectroscopy, Biophys. J. 32 (1980) 1007–1021.
[26] J.M. Boggs, Lipid intermolecular hydrogen bonding: influence on structural organization and membrane function, Biochim. Biophys. Acta 906 (1987) 353–404.
[27] M.J. Ruocco, D.J. Siminovitch, J.R. Long, S.K. Das Gupta, R.G. Griffin, ^{2}H and ^{13}C nuclear magnetic resonance study of *N*-palmitoylgalactosylsphingosine (cerebroside)/cholesterol bilayers, Biophys. J. 71 (1996) 1776–1788.
[28] J.S. O'Brien, Stability of the myelin membrane, Science 147 (1965) 1099–1107.
[29] S. Ali, H.L. Brockman, R.E. Brown, Structural determinants of miscibility in surface films of galactosylceramide and phosphatidylcholine: effect of unsaturation in the galactosylceramide acyl chain, Biochemistry 30 (1991) 11198–11205.
[30] S. Ali, J.M. Smaby, R.E. Brown, Galactosylceramides with homogeneous acyl chains: the effect of acyl structure on intermolecular interactions occurring at the argon/buffered saline interface, Thin Solid Films 244 (1994) 860–864.
[31] J.M. Smaby, V.S. Kulkarni, M. Momsen, R.E. Brown, The interfacial elastic packing interactions of galactosylceramides, sphingomyelins, and phosphatidylcholines, Biophys. J. 70 (1996) 868–877.
[32] J.M. Smaby, M. Momsen, V.S. Kulkarni, R.E. Brown, Cholesterol-induced interfacial area condensations of galactosylceramides and sphingomyelins with identical acyl chains, Biochemistry 35 (1996) 5696–5704.
[33] D. Singh, J.H. Davis, C.W.M. Grant, Behaviour of a glycosphingolipid with unsaturated fatty acid in phosphatidylcholine bilayers, Biochim. Biophys. Acta 1107 (1992) 23–30.
[34] M.R. Morrow, D. Singh, C.W.M. Grant, Glycosphingolipid acyl chain order profiles: substituent effects, Biochim. Biophys. Acta 1235 (1995) 239–248.
[35] R.A. Reed, G.G. Shipley, Effect of chain unsaturation on the structure and thermotropic properties of galactocerebrosides, Biophys. J. 55 (1989) 281–292.

[36] N.S. Haas, G.G. Shipley, Structure and properties of *N*-palmitoleoylgalactosylsphingosine (cerebroside), Biochim. Biophys. Acta 1240 (1995) 133–141.
[37] D.D. Archibald, S. Mann, Self-assembled microstructures from 1,2-ethanediol suspensions of pure and binary mixtures of neutral and acidic biological galactosylceramides, Chem. Phys. Lipids 69 (1994) 51–64.
[38] V.S. Kulkarni, W.H. Anderson, R.E. Brown, Bilayer nanotubes and helical ribbons formed by hydrated galactosylceramides: acyl chain and headgroup effects, Biophys. J. 69 (1995) 1976–1986.
[39] L.D. Mayer, M.J. Hope, P.R. Cullis, A.S. Janoff, Solute distributions and trapping efficiencies observed in freeze-thawed multilamellar vesicles, Biochim. Biophys. Acta 817 (1985) 193–196.
[40] F.P. Schwarz, Biological thermodynamic data for the calibration of differential scanning calorimeters: dynamic temperature data on the gel to liquid crystalline phase transition of dialkylphosphatidylcholine in water suspensions, Thermochim. Acta 177 (1991) 285–303.
[41] R. Koynova, M. Caffrey, Phases and phase transitions of the sphingolipids, Biochim. Biophys. Acta 1255 (1995) 213–236.
[42] L.-K. Li, L. So, A. Spector, Age-dependent changes in the distribution and concentration of human lens cholesterol and phospholipids, Biochim. Biophys. Acta 917 (1987) 112–120.
[43] G.L. Pennacchiotti, N.P. Rotstein, M.I. Aveldano, Effects of clofibrate on lipids and fatty acids of mouse liver, Lipids 31 (1996) 179–185.
[44] S.K. Kundu, I. Diego, S. Osovitz, D.M. Marcus, Glycosphingolipids of human plasma, Arch. Biochem. Biophys. 238 (1985) 388–400.
[45] S. Li, J. Chien, C. Wan, Y. Li, Occurrence of glycosphingolipids in chicken egg yolk, Biochem. J. 173 (1978) 697–699.
[46] J.L. Foote, E. Coles, Cerebrosides of human aorta: isolation, identification of the hexose, and fatty acid distribution, J. Lipid Res. 9 (1968) 482–486.
[47] J.B. Speyer, R.T. Weber, S.K. Das Gupta, R.G. Griffin, Anisotropic ^{2}H NMR spin-lattice relaxation in Lα-phase cerebroside bilayers, Biochemistry 28 (1989) 9569–9574.
[48] I. Pascher, M. Lundmark, P.-G. Nyholm, S. Sundell, Crystal structures of membrane lipids, Biochim. Biophys. Acta 1113 (1992) 339–373.
[49] K.S. Hamilton, H.C. Jarrell, K. Briere, C.W.M. Grant, Glycosphingolipid backbone conformation and behavior in cholesterol-containing phospholipids bilayers, Biochemistry 32 (1993) 4022–4028.
[50] R.H. Pearson, I. Pascher, The molecular structure of lecithin dihydrate, Nature 281 (1979) 499–501.
[51] M. Gardam, J.R. Silvius, Intermixing of dipalmitoylphosphatidylcholine with phospho- and sphingolipids bearing highly asymmetric hydrocarbon chains, Biochim. Biophys. Acta 980 (1989) 319–325.
[52] D.A. Pink, A.L. MacDonald, B. Quinn, Anisotropic interactions in hydrated cerebrosides. A theoretical model of stable and metastable states and hydrogen-bond formation, Chem. Phys. Lipids 47 (1988) 83–95.
[53] I.R. Miller, D. Bach, Effect of ethylene glycol on the phase transition kinetics of gluco- and galactocerebrosides, Biochim. Biophys. Acta 863 (1986) 121–127.
[54] G. Lagaly, A. Weiss, E. Stuke, Effect of double-bonds on bimolecular films in membrane models, Biochim. Biophys. Acta 470 (1977) 331–341.
[55] S. Ali, J.M. Smaby, R.E. Brown, Acyl structure regulates galactosylceramide's interfacial interactions, Biochemistry 32 (1993) 11696–11703.
[56] C. Huang, S. Li, Z.-q. Wang, H. Lin, Dependence of the bilayer phase transition temperatures on the structural parameters of phosphatidylcholines, Lipids 28 (1993) 365–370.
[57] S. Li, Z. Wang, H. Lin, C. Huang, On the main phase transition temperatures of highly asymmetric mixed-chain phosphatidylcholines, Biochim. Biophys. Acta 1194 (1994) 271–280.
[58] G. Wang, H. Lin, S. Li, C. Huang, Phosphatidylcholines with *sn*-1 saturated and *sn*-2 *cis* monounsaturated acyl chains, J. Biol. Chem. 270 (1995) 22738–22746.
[59] J.M. Boggs, K.M. Koshy, G. Rangaraj, Interdigitated lipid bilayers of long acyl chain species of cerebroside sulfate. A fatty acid spin label study, Biochim. Biophys. Acta 938 (1988) 373–385.
[60] T.J. McIntosh, S.A. Simon, D. Needham, C. Huang, Structure and cohesive properties of sphingomyelin/cholesterol bilayers, Biochemistry 31 (1992) 2012–2020.
[61] P.R. Maulik, G.G. Shipley, X-Ray diffraction and calorimetric study of N-lignoceryl sphingomyelin membranes, Biophys. J. 69 (1995) 1909–1916.
[62] J.T. Mason, C. Huang, R.L. Biltonen, Calorimetric investigations of saturated mixed-chain phosphatidylcholine bilayer dispersions, Biochemistry 20 (1981) 6086–6092.
[63] C. Huang, J.T. Mason, Structure and properties of mixed-chain phospholipid assemblies, Biochim. Biophys. Acta 864 (1986) 423–470.
[64] P.R. Maulik, G.G. Shipley, Interactions of N-stearoyl sphingomyelin with cholesterol and dipalmitoylphosphatidylcholine in bilayer membranes, Biophys. J. 70 (1996) 2256–2265.
[65] V.S. Kulkarni, R.E. Brown, Modulation of tubular microstructural self-assembly in galactosylceramide: influence of N-linked fatty acyl chains, Proc. Microsc. Microanal. 1996 (1996) 936–937.
[66] A.S. Goldstein, A.N. Lukyanov, P.A. Carlson, P. Yager, M.H. Gelb, Formation of high-axial-ratio-microstructures from natural and synthetic sphingolipids, Chem. Phys. Lipids 88 (1997) 21–36.
[67] P.-G. Nyholm, I. Pascher, Orientation of the saccharide chains of glycolipids at the membrane surface: conformational analysis of the glucose-ceramide and the glucose-glyceride linkages using molecular mechanics (MM3), Biochemistry 32 (1993) 1225–1234.
[68] K.S. Bruzik, P.-G. Nyholm, NMR study of the conformation of galactocerebroside in bilayers and solution: galactose

reorientation during the metastable-stable gel transition, Biochemistry 36 (1997) 566–575.
[69] V.S. Kulkarni, R.E. Brown, Thermotropic behavior of galactosylceramides with monounsaturated fatty acyl chains, Biophys. J. 72 (1997) A401.
[70] J.M. Boggs, K.M. Koshy, G. Rangaraj, Influence of structural modifications on the phase behavior of semi-synthetic cerebroside sulfate, Biochim. Biophys. Acta 938 (1988) 361–372.